Characterization of Susceptibility Artifacts in MR-thermometry PRFS-based during Laser Interstitial Thermal Therapy

Martina De Landro
Department of Mechanical Engineering
Politecnico di Milano
Milan, Italy
martina.delandro@polimi.it

Céline Giraudeau
IHU Strasbourg
Institute of Image-guided Surgery
Strasbourg, France
celine.giraudeau@ihu-strasbourg.eu

Juan Verde
IHU Strasbourg
Institute of Image-guided Surgery
Strasbourg, France
juan.verde@ihu-strasbourg.eu

Khalid Ambarki
Siemens Healthcare SAS
Saint-Denis, France
khalid.ambarki@siemens-healthineers.com

Henrik Odéen
School f Medicine
University of Utah
Salt Lake City, Utah, USA
henrik.odeen@hsc.utah.edu

Benoit Gallix
IHU Strasbourg
Institute of Image-guided Surgery
Strasbourg, France
benoit.gallix@ihu-strasbourg.eu

Paola Saccomandi
Department of Mechanical Engineering
Politecnico di Milano
Milan, Italy
paola.saccomandi@polimi.it

Abstract— **Magnetic Resonance Thermometry (MRT) is demonstrating huge abilities to guide laser interstitial thermal therapy (LITT) in several organs, such as the brain. Among the methods to perform MRT, Proton Resonance Frequency (PRF) shift holds significant benefits, like tissue independence. Despite its potential, PRF shift-based MRT holds significant challenges affecting the accuracy of reconstructed temperature maps. In particular, susceptibility artifacts due to gas-bubble formation are an important source of error in temperature maps in MRT-guided LITT. This work presents the characterization of the susceptibility artifacts in MRT-guided LITT and the measurement of its size. LITT was performed in gelatin-based phantoms, at 5 W, 2 W, 1 W, and 0.5 W under MRI guidance with a 1.5 T clinical MRI scanner. Temperature images were obtained with a 3D EPI (Echo-planar imaging) prototype sequence. Areas of temperature errors were defined as zones of negative temperature variation <-2 °C. Moreover, we have analyzed the artifact shape in sagittal, axial and coronal planes. The analysis demonstrates a double-lobe shape for the susceptibility artifact mainly distributed in the sagittal plane. Also, the higher laser power caused a bigger artifact area. Temperature errors of ~80 °C proved the necessity to avoid susceptibility artifact generation during MRT-guided LITT. The analysis of the influence of the laser power on the artifact has suggested that using low laser power (0.5 W) helps avoid this measurement error.**

Keywords— Magnetic Resonance Thermometry, susceptibility artifacts, laser interstitial thermal therapy

I. INTRODUCTION

Magnetic Resonance Thermometry (MRT) has been proposed to intraoperatively guide laser interstitial thermal therapy (LITT) thanks to its ability to provide multidimensional temperature measurements [1, 2]. MRT-guided LITT is a surgical procedure mainly utilized in the treatment of intracranial pathologies to selectively treat a lesion using heat generated from laser-tissue interaction [3, 4]. During MR-guided LITT, the system software utilizes the measured temperature distribution to predict the thermal damage giving an estimation of the damage boundaries in real-time. Most of the applications of MRT rely on the proton resonance frequency (PRF) shift method. The shift in the proton resonance is due to changes in intermolecular hydrogen bonding, caused by the temperature variation of the medium. This shift is directly proportional to the change of tissue temperature; hence it can be used to compute the temperature increase pixel-by-pixel [1, 6]. The PRF shift method is applicable for the temperature range of interest for the thermal therapies, i.e., 20 – 100 °C, and holds the advantage of being tissue-nonspecific for most of the soft tissues. Beyond the abovementioned benefits, some sources of errors, including susceptibility artifacts, can affect the accuracy of temperature maps [7, 8]. Phase shift in MR images is also produced by time-dependent variations in the tissue magnetic susceptibility. The interaction between the laser light and the tissue causes the creation of cavitation bubbles, which in turn provoke artifacts on the thermometric image. Gas bubbles produce magnetic susceptibility contrast, which is increased by 9 ppm over the typical values for biological tissue, and the PRF shift MRT is not able to discern the effect of the temperature-induced chemical shift from changes in the local magnetic field [9]. These artifacts can impair the accurate temperature measurement inside and around the target lesion [9, 10]. Moreover, measurement errors, such as drift of the magnetic field under temperature change and motion, still represent an important source of uncertainty in the temperature measurement (the uncertainty is recommended to be lower than

1-2 °C) even though several approaches, such as algorithms for motion compensation and magnetic field drift correction, have been proposed to mitigate these last two drawbacks [11].

In this work, we characterize the LITT-induced artifact in MRT images. We propose a method to measure the dimension of susceptibility artifacts in MRT-guided LITT within a homogeneous target. We also investigate the shape of the artifact in the three planes (axial, coronal, and sagittal), together with the relationship between the artifact size and the laser power.

II. MATERIALS AND METHODS

A. MRT-guided LITT

A homogeneous and isotropic material, mimicking the thermal properties of biological tissue, was selected to carry out our analysis [12, 13, 14]. We choose to work with a transparent medium, to make visible the effects of the laser and the formation of the bubbles. To this aim, a porcine-based gelatine phantom underwent LITT using a laser diode (975 nm, LuOcean Mini 4, Lumics, Berlin, Germany) delivering radiation to an MR-compatible fiber applicator (400 μm, THORLABS, Dachau, Germany) (Fig. 1). The laser applicator was set to deliver a power of 0.5, 1, 2, and 5 W for 5 minutes. After the laser was turned off, the cooling phase was also recorded for 2 minutes.

LITT was performed under MRI guidance with a 1.5 T clinical MRI scanner (Siemens Magnetom Aera, Erlangen, Germany). We used spine coil and flex surface coil on the phantom, and temperature images were obtained with a 3D EPI (Echo-planar imaging) prototype sequence [5]. Ten slices were placed in the axial, coronal, and sagittal orientations thus allowing a comprehensive analysis of the artifact shape in space and time. Three experiments were performed for each power value, on different locations of the phantom. The protocol has been defined in order to adapt the field of view to the phantom and have a suitable spatial and time resolution [15]. The following parameters were used:

- field of view 300 mm x 300 mm;

- phase resolution 50%; in-plane resolution 1.4 mm x 2.8 mm; reconstructed resolution 1.4 mm x 1.4 mm;

- slice thickness 3 mm; 10 slices;

- TE/TR=11 ms/24 ms;

- flip angle 10°;

- EPI factor 7;

- 20 baseline averages to reach equilibrium magnetization;

- temporal resolution 3.62 s;

- 135 measurements leading to 8 minutes of total acquisition time.

Real-time visualization of the temperature maps was enabled by the Certis Solution software (Certis Therapeutics, France).
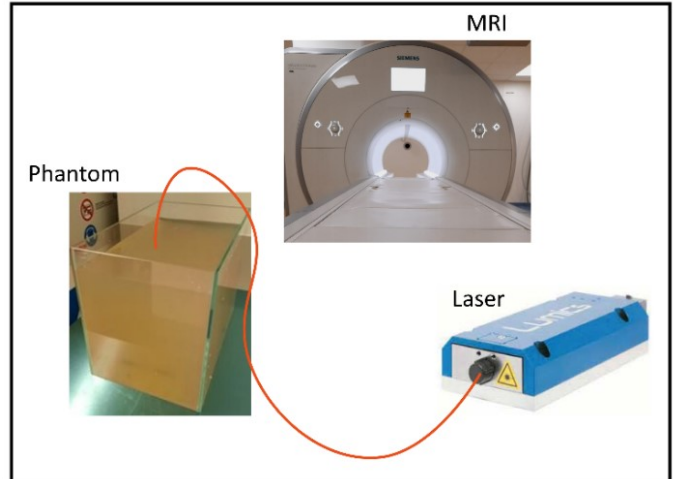

Fig. 1. Schematic of the experimental setup. The porcine-based gelatine phantom was irradiated using bare optical fiber (orange) properly placed in the medium using an MRI-compatible needle. LITT was performed under MRI guidance and real-time temperature change during the experiments was measured using a 3D segmented EPI prototype sequence.

B. Image analysis

The data analysis was carried out on Matlab R2020a. Before undertaking the artifact investigation, other potential sources of measurement uncertainty were removed. In particular, the correction of the B_0 drift was performed by subtracting to the whole image the signal of a reference area selected in a location of the phantom which is not affected by the temperature change [9]. Artifacts in the images were masked using a thresholding operation. Artifact region was defined as the area of negative temperature variation causing misleading temperature reconstruction in the images. Areas of temperature errors were defined as zones of negative temperature variation (<-2 °C). Knowing the size of the pixels, we could estimate the area of the artifacts, in all the planes in which it was appreciable. Two areas were calculated: the area in each slice, and the cumulative area, which is given by the sum of the areas in all the slices. The susceptibility artifacts were characterized following three steps: 1) analysis of the artifact shape in the three planes for the experiment at 2 W; 2) investigation of the artifact dimension dependence with laser power; 3) quantification of the temperature errors in the artifact area.

III. RESULTS AND DISCUSSION

Fig. 2 shows the LITT outcomes in the gelatine phantom, for the three power values causing artifacts in the MRT images. Gas-bubbles causing errors in the measured temperature are clearly visible, with higher power resulting in larger damaged area and bubbles zone.
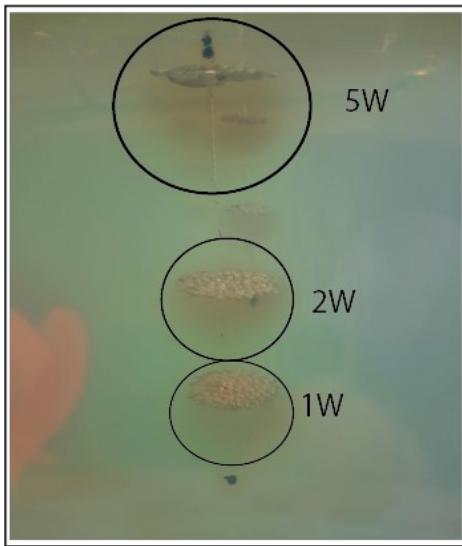
Fig. 2. Example of LITT outcomes for the three power values leading gas-bubble formation: 1 W, 2 W and 5 W.

A. Analysis of the artifact shape at 2 W

Temperature maps acquired in the three planes are reported in Fig. 3 (Fig. 3a, axial plane; Fig. 3b, coronal plane; Fig. 3c sagittal plane). Studying the artifact formation in the three planes, different views of the same shape are distinguished, and a double-lobe appearance mainly distributed in the sagittal plane is visible.
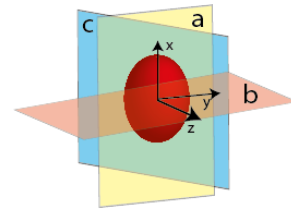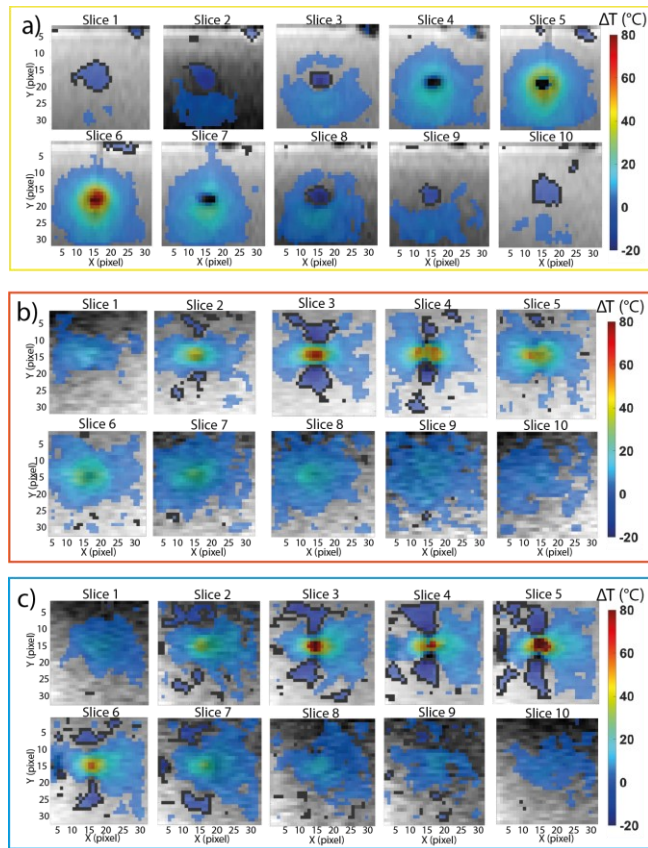

Fig. 3. Maps of temperature change measured for the 10 slices at the time instant corresponding at the maximum temperature increase (~5min) in the 2 W case for a) axial (yellow), b) coronal (orange) and c) sagittal (blue) planes. The artifact area is reported as the zone of negative temperature variation (<-2 °C), dark blue regions with black boundaries in the images. A maximum temperature increase of 80 °C was measured for this experiment.

The maximum temperature induced by LITT is 80 °C, as observable in the slice no. 5 of the sagittal plane (Fig. 3c). This result shows that the choice of the plane is crucial also for the correct measurement of the target temperature.

The slice presenting the biggest artifact was selected for each plane (Fig. 4a), and the artifact's evolution in time was measured. We can observe that the lobes' structure mainly extends in the sagittal plane. The artifact area increases with a trend similar to the one of the phantom temperature. The maximum value is recorded at 5 min for the sagittal plane. Also, the total area of pixels defined as susceptibility artifact regions in the 10 slices along the time, shows the higher value of ~25 cm² for the sagittal plane (Fig. 4b).
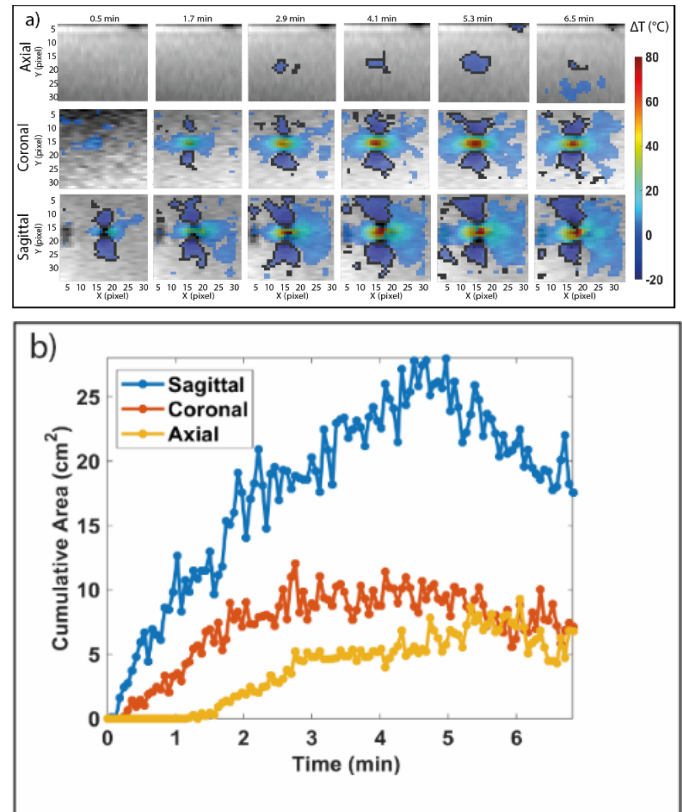

Fig. 4. a) Temperature maps highlighting artifact evolution in time in the three planes. Results are reported for slices no. 1, 3, and 4 showing the biggest artifact area for the axial, coronal, and sagittal planes, respectively, at several time steps

of the LITT. b) Cumulative area measured as the sum of the pixels labeled in the images as artifact for the 10 slices in time and for sagittal (blue), coronal (orange), and axial (yellow) views.

B. Artifact dimension dependence with power settings

Gas bubbles were formed in the experiments performed with power > 0.5 W (Fig. 2). Results of the power-artifact dimension relationship are shown in Fig. 5. In this case, the sagittal plane holding most of the area of error information was considered sufficient for the artifact description. Both the artifact area at a set time (Fig. 5a) and the temporal evolution of cumulative area (Fig. 5b) indicate higher values by increasing power on average. The largest artifact area is always found in the central slices (between slices no. 4 to no. 6, Fig. 5a). At 5 W, the maximum cumulative area after 5 minutes of LITT reaches 39 cm^2, whereas it remains < 10 cm^2 when 1 W was used (Fig. 5b).

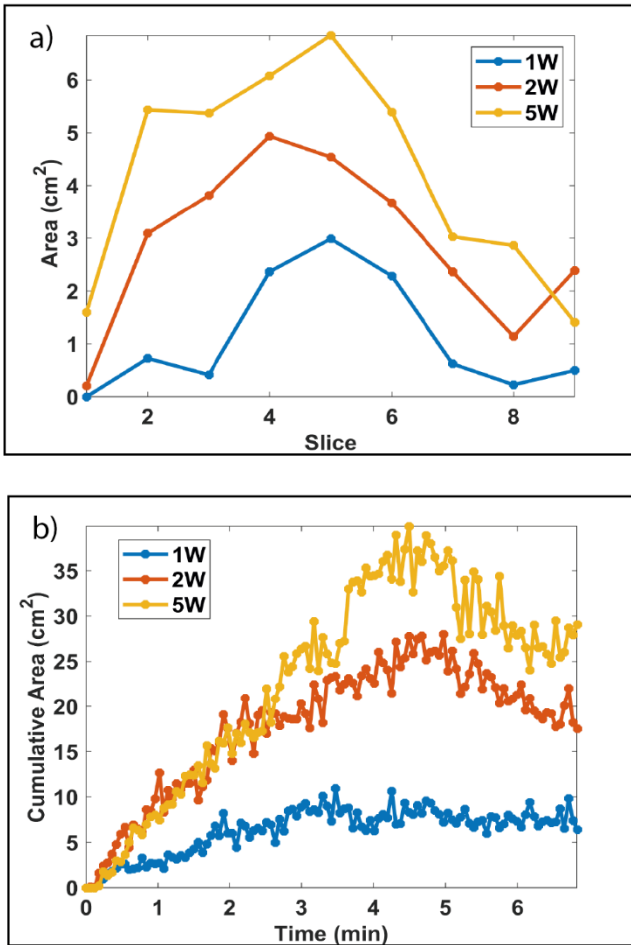Fig. 5. a) Artifact area estimated in the sagittal plane for the LITT performed at 1 W (blue), 2 W (orange) and 5 W (yellow). Area values in cm^2 are shown for the 10 slices in the time instant revealing the maximum artifact occurrence (~ 5 min). b) Cumulative area during the procedure for 1 W, 2 W and 5 W experiments.

C. Temperature error in the artifact area

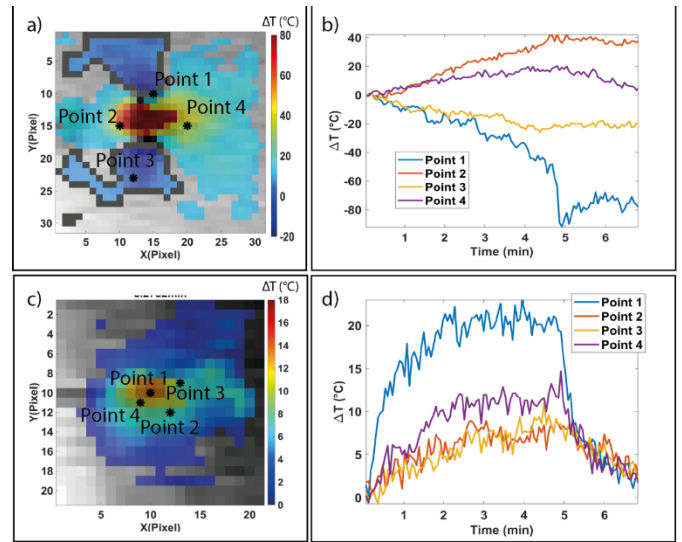Fig. 6 shows a pixel-based analysis of the artifact.

Fig. 6. a) Selected points in the MRT images for the experiment at 2 W in the sagittal plane. b) Temperature evolution extracted for the chosen pixels when the artifact is present. c) Selected points in the MRT images for the experiment at 0.5 W in the sagittal plane. d) Temperature evolution extracted for the chosen pixels without any susceptibility artifact.

To quantify the temperature error caused by the artifact formation, 4 pixels were selected in the MRT images (Fig. 6a), and the corresponding temperature profiles are displayed in Fig. 6b. In the artifact area (Point 1 and Point 3), a negative temperature variation is measured which can reach a minimum value of -80 °C at the end of ablation. On the other hand, at 0.5 W (Fig. 6c-d), temperature evolution for the artifact-absence case enables an accurate 2D thermal map reconstruction in real-time.

IV. DISCUSSION AND CONCLUSIONS

MRT is a useful solution for real-time thermometry during thermal therapies, as demonstrated by the clinical applications for the minimally invasive treatment of tumors [4]. However, this measurement technique still requires several improvements regarding the minimization of measurement uncertainties which are mainly related to motion (e.g., breathing motion, tremor, etc.) and changes in the local magnetic field. Indeed, MRT based on PRF shift has shown substantial sensitivity to local magnetic field changes ascribable to transient cavitation phenomena. This high sensitivity causes a consistent temperature error in the images.

Viallon and colleagues have analyzed a similar phenomenon, caused by another electromagnetic source, *i.e.*, radiofrequency [9], and proposed a model to correct the artifact for their specific settings. Even though the problem is well known also in clinical practice [7], only a few studies have proposed a deeper investigation of this aspect.

In our work, we have carried out the first characterization of the observed transient cavitation artifact, in both space and time, during LITT. We have observed that the artifact, which is constituted by two main lobes centred on the source, is big in sagittal plane (it can reach 7 cm^2 after 5 minutes-LITT in the central slice, as shown in Fig. 5a). As expected, the area

concerned by the artifact increases with the laser power. This phenomenon is particularly noticeable when the power density is high. Indeed, in our experiments, we have used a standard bare fiber applicator with a diameter of 0.3 mm. As a result, low power (0.5 W, in our case) firstly consists of an implementable solution to avoid those susceptibility artifacts. For some therapeutic applications, such as MRT-guided LITT for brain tumor treatment, different applicators are used, such as water-cooled fibers with diffusive tips. Here, due to systems working differently, laser powers higher than the ones we used (from 10 W to 20 W, even 30 W) did not always report artifacts [16, 17]. These results suggest that prior characterization of the laser delivery system is crucial to minimize artifacts in MRT and errors in thermal damage estimate.

As a corollary, it could be interesting to investigate the effect of a gradually increasing power during the ablation to assess if the generation of gas bubbles could be mitigated, thus controlling artifact occurrence.

We chose here the PRF shift method even though it cannot distinguish the effect of temperature-induced chemical shift change from pre-operatory changes in the local magnetic field, as it remains the technique mostly used with modern laser ablation systems. The other available methods in MRI encounter tissue-dependent signal change that interferes with accurate temperature monitoring and were proved to be less sensitive and accurate [18].

The main limitation of our study, which leaves space to further improvements, regards the use of a homogeneous gelatine phantom and consequently does not take into account the effect of blood flow in living tissues, which has the potential to divert heat away from the target zone. In future work, we will investigate the influence of laser power on perfused tissues.

REFERENCES

[1] H. Odéen, D. L. Parker, "Improved MR thermometry for laser interstitial thermotherapy," Lasers Surg Med, vol. 51, no. 3, pp. 286-300, 2019.

[2] M. De Landro, J. Ianniello, M. Yon, A. Wolf, B. Quesson, E. Schena, and P. Saccomandi, "Fiber bragg grating sensors for performance evaluation of fast magnetic resonance thermometry on synthetic phantom". Sensors, vol. 20, no. 22, pp. 6468, 2020.

[3] A. M. Mohammadi, J. L. Schroeder, "Laser interstitial thermal therapy in treatment of brain tumors – the NeuroBlate System". Expert Rev. Med. Devices, vol. 11, pp. 109–119, 2014.

[4] Salem U, Kumar VA, Madewell JE, D.F. Schomer, D. Bastos, P. O. Zinn, J.S. Weinberg, et al, "Neurosurgical applications of MRI guided laser interstitial thermal therapy (LITT), " Cancer Imaging vol. 19, no. 1, pp. 1-13, 2019.

[5] M. De Landro M, S. Korganbayev, K. Ambarki, J. Verde, H. Odeen, C. Giraudeau, P. Saccomandi, "Magnetic resonance-based measurement system: comparison of 2D and 3D echo-planar imaging sequences for thermometry application," 2021 IEEE International Instrumentation and Measurement Technology Conference (I2MTC); pp. 1–6, 2021.

[6] L. Winter, E. Oberacker, K. Paul, Y. Ji, C. Oezerdem, P. Ghadjar, et al., "Magnetic resonance thermometry: Methodology, pitfalls and practical solutions," Int. J. Hyperth. vol. 32, no. 1, pp. 63-75, 2016.

[7] S.M. Munier, A.S. Liang, A. N. Desai, J. K. James, S. F. Danish, "Characterization of Magnetic Resonance Thermal Imaging Signal Artifact During Magnetic Resonance Guided Laser-Induced Thermal Therapy," Operative Neurosurgery, vol. 19, no. 5, pp. 619-624, 2020.

[8] N. D. Schulmann, M. Soltani-Sarvestani, M. De Landro, S. Korganbayev, S. Cotin, P. Saccomandi, "Model-Based Thermometry for Laser Ablation Procedure Using Kalman Filters and Sparse Temperature Measurements," IEEE Transactions on Biomedical Engineering, 2022, doi: 10.1109/TBME.2022.3155574.

[9] M. Viallon, S. Terraz, J. Roland, E. Dumont, C. D. Becker, R. Salomir, "Observation and correction of transient cavitation‐induced PRFS thermometry artifacts during radiofrequency ablation, using simultaneous Ultrasound/MR imaging," Medical physics, vol. 37, no. 4, pp. 1491-1506, 2010.

[10] H. Odéen, D. L. Parker, "Magnetic resonance thermometry and its biological applications–Physical principles and practical considerations," Progress in nuclear magnetic resonance spectroscopy, vol. 110, pp. 34-61, 2019.

[11] D. Fuentes, J. Yung, J. D. Hazle, J. S. Weinberg, R. J. Stafford, "Kalman filtered mr temperature imaging for laser induced thermal therapies," IEEE Transactions on Medical Imaging, vol. 31, no. 4, pp. 984–994, 2012.

[12] F. Morra, M. De Landro, S. Korganbayev, A. Wolf, A Dostovalov, A. Cigada, P. Saccomandi, "Spatially resolved thermometry during laser ablation in tissues: Distributed and quasi-distributed fiber optic-based sensing," Optical Fiber Technology, vol. 58, no. 112295, 2020.

[13] L. Bianchi, F. Cavarzan, L. Ciampitti, M. Cremonesi, F. Grilli, P. Saccomandi, "Thermophysical and mechanical properties of biological tissues as a function of temperature: a systematic literature review," International Journal of Hyperthermia, vol. 39, no. 1, pp. 297-340, 2022.

[14] S. Asadi, S. Korganbayev, W. Xu, A. K. Mapanao, V. Voliani, V-P. Lehto, P. Saccomandi, "Experimental Evaluation of Radiation Response and Thermal Properties of NPs-Loaded Tissues-Mimicking Phantoms," Nanomaterials, vol. 16, no. 2, pp. 945, 2022.

[15] G. Andria, F. Attivissimo, G. Cavone, A. M. L. Lanzolla, "Acquisition Times in Magnetic Resonance Imaging: Optimization in Clinical Use," IEEE Transactions on Instrumentation and Measurement, vol. 58, no. 9, pp. 3140-3148, 2009.

[16] S.M. Munier, E.L. Hargreaves, N.V. Patel, S.F. Danish, "Effects of variable power on tissue ablation dynamics during magnetic resonance-guided laser-induced thermal therapy with the Visualase system," International Journal of Hyperthermia, vol. 34, no. 6, pp. 764-772, 2018.

[17] A.S. Liang, S.M. Munier, S.F. Danish, "Controlling signal artifact with software threshold imaging for magnetic resonance-guided laser interstitial thermal therapy. Operative Neurosurgery (Hagerstown), vol. 22, no. 2, pp. 75-79, 2022.

[18] B. Bazrafshan, et al. "Temperature imaging of laser-induced thermotherapy (LITT) by MRI: evaluation of different sequences in phantom," Lasers in Medical Science, vol. 29, no. 1, pp. 173-183, 2014.